Published in final edited form as:
Chemosphere. 2017 April ; 173: 245–252. doi:10.1016/j.chemosphere.2017.01.050.

Nanosilver as a disinfectant in dental unit waterlines: Assessment of the physicochemical transformations of the AgNPs

Alireza Gitipour[a], **Souhail R. Al-Abed**[b], **Stephen W. Thiel**[a], **Kirk G. Scheckel**[b], and **Thabet Tolaymat**[b]

[a]Biomedical, Chemical, and Environmental Engineering, University of Cincinnati, Cincinnati, OH, USA

[b]US EPA, Office of Research and Development, National Risk Management Laboratory, Cincinnati, OH, USA

Abstract

Dental unit water lines (DUWL) are susceptible to biofilm development and bacterial growth leading to water contamination, causing health and ecological effects. This study monitors the interactions between a commonly used nanosilver disinfectant (ASAP-AGX-32, an antimicrobial cleaner for dental units, 0.0032% Ag) and biofilm development in DUWL. To simulate the disinfection scenario, an in-house DUWL model was assembled and biofilm accumulation was allowed. Subsequent to biofilm development, the disinfection process was performed according to the manufacturer's instructions. The pristine nanosilver particles in the cleaner measured between 3 and 5 nm in diameter and were surrounded by a stabilizing polymer. However, the polymeric stabilizing agent diminished over the disinfection process, initiating partial AgNPs aggregation. Furthermore, surface speciation of the pristine AgNPs were identified as primarily AgO, and after the disinfection process, transformations to AgCl were observed. The physicochemical characteristics of AgNPs are known to govern their fate, transport and environmental implications. Hence, knowledge of the AgNPs characteristics after the disinfection process (usage scenario) is of significance. This study demonstrates the adsorption of AgNPs onto biofilm surfaces and, therefore, will assist in illustration of the toxicity mechanisms of AgNPs to bacteria and biofilms. This work can be an initial step in better understanding how AgNPs transform depending on the conditions they are exposed to during their lifetime. Until this date, most research has been focused on assessing the impacts of pristine (lab synthesized) nanomaterials on various systems. However, it is our belief that nanoparticles may undergo transformations during usage, which must be taken into consideration. Furthermore, this experiment is unique as it was conducted with a commonly used, commercially available nanosilver suspension leading to more realistic and applicable findings.

1. Introduction

In recent times, nanomaterials have found applications in many aspects of our daily life. They have been progressively incorporated into a wide range of consumer products. Paints, textiles, personal care products, medical apparatus, batteries, and sporting goods are just a few examples of such products currently available in the market. Attributed to their size,

nanomaterials have shown to display specific characteristics such as high surface-to-volume ratio and higher reactivity in comparison to the bulk material. Today, nanomaterials are synthesized utilizing various techniques and methods leading to an extensive variety of nanomaterials encompassing different characteristics.

The widespread use of nanomaterials in commercial products may lead to their release and accumulation in the environment (e.g., soil and water) (Hajipour et al., 2012). Depending on the inherent nature and characteristics of the nanomaterial, environmental exposure may lead to negative ecological impacts. Silver nanoparticles, which are well-known and primarily utilized for their antibacterial and antifungal properties, are currently the most extensively used nanomaterial in consumer products (Tolaymat et al., 2010). In the case of silver nanoparticles (AgNPs), based on their antibacterial characteristics, there is concern regarding their possible impacts on beneficial microbial communities in the ecosystem and also waste management processes that heavily depend on microbial degradation (Donoso-Bravo et al., 2011).

Microbial and biofilm growth in water delivery lines are a persistent problem facing the dental industry (Costa et al., 2016). Typically, dental unit waterlines contain opaque, small-diameter tubing that carry water to and from the patient's mouth during dental procedures. Due to their small inner diameter and composition, mainly flexible polyurethane or other plastics, dental lines are an excellent environment for the development of microbial biofilms. The inner surface of the dental tubing acts as a substrate, allowing bacteria to use the hardeners and additives as a nutrient source promoting biofilm growth (Walker and Marsh, 2007). The biofilm and bacteria will eventually percolate into the water stream, posing health risks to patients, as well as dental health care personnel (Szymanska, 2003). Occupational asthma has been reported as a potential risk factor dental staff face from inhalation of aerosolsgenerated from the biofilm contaminated dental unit waterlines (Pankhurst et al., 2005). Also, the biofilm cause a foul odor and are known to give water a bad taste (Shepherd et al., 2001).

In light of the above, a clean water delivery system is essential for dental procedures. In the past, instruments such as ultrasonic scalers were utilized for reducing the growth of microorganisms (Blake, 1963). Other more common methods used for preventing contamination include installation of independent water systems, water filtration and sterilization systems or a variety of chemical treatment protocols (Pankhurst et al., 1998). It is important to note that sterile water delivery systems have proven to be expensive to purchase, maintain and less convenient to use compared to the conventional water delivery systems (Shearer, 1996). As for chemical treatments, a variety of chemicals have been examined for their decontamination capability against these microorganisms and biofilms (e.g. hydrogen peroxide, ethanol and ozone). Dependent on the intrinsic nature of the chemical agents, the application procedures vary, ranging from intermittent use to continuous introduction to the water supply. However, the potential implications of the chemical treatments on different components of the dental unit, and their biochemical interactions are not always known or predictable (Pankhurst et al., 1998). Therefore, it is important to investigate the safety and efficacy of chemical treatments to ensure patient and dental personnel protection.

AgNPs have been established as a beneficial disinfecting agent with applications in countless fields. In dentistry, AgNPs are utilized as a means to prevent or reduce biofilm growth over dental material surfaces (Correa et al., 2015). As an example, numerous nanosilver solutions are commercially available for the disinfection of dental unit waterlines. The dental lines are routinely flushed with a nanosilver solution for a duration of time, rinsed, and brought back into service. Although this practice has gained popularity, little research has been conducted assessing the physicochemical transformations of the AgNPs during the disinfection process, and more importantly, upon exiting the system.

The objective of this research was to investigate the physicochemical alterations of commercial nanosilver cleaner (ASAP-AGX-32, an antimicrobial cleaner for dental units, 0.0032% Ag) as a disinfectant on biofilm growth in dental unit water lines (DUWL). It is well established that the physicochemical properties (e.g. aggregation, complexations, and transformations) of nanosilver govern their fate, as well as their potential environmental implications. However, this observation has been primarily evaluated using fresh laboratory-synthesized AgNPs. Lab-synthesized AgNPs may possess different characteristics compared to AgNPs in consumer products attributed to factors such as aging (shelf-life), matrix used (e. g., dispersants, additives, etc.) and exposure to light. Hence, it is our goal to simulate the disinfection process commonly utilized by dental offices and monitor the alterations to the physicochemical properties of the commercially available AgNPs under real life circumstances.

2. Experimental methodology

An in-house DUWL model was built to simulate common dental unit water lines used in dental practices. A continuous flow system of tap water was utilized as shown in Fig. S1. Gray polyurethane tubing with an outer diameter of 1/4″ was purchased from 55 Dental Supplies and Equipment (www.55dental.com) and used for this experiment. The model was designed to allow tap water to run through multiple loops of dental tubing and ultimately drain into a collection tank. As water was siphoned from the tank, it was automatically replaced using a float valve, allowing unattended continuous water flow. The continuous water flow rate was set at 2 mL min^{-1} and a total of twelve 4 m in length dental tubing lines were utilized. After 5.5 months of continuous tap water circulating through the DUWL, a substantial accumulation of biofilm was detected according to the microbial analysis. At this time, the dental tubing was transferred to the re-circulating disinfection system (Fig. S2) and 2 ppm nanosilver was circulated through the system for a duration of 3 days following the manufacturer's instructions.

Figure S2 is a schematic of the setup used for the disinfection process. Two liters of commercial nanosilver cleaner ASAP-AGX-32 (0.0032% Ag) were prepared with a final silver concentration of 2 ppm to be used for the course of the disinfection process. Initially, 1.5 L of the diluted nanosilver solution was added to bottle A and 0.5 L to bottle B. The flow rate from bottle A to B was set at 1.3 mL s^{-1} for a 10 min interval resulting in 800 mL of solution transferring from A to B. After 10 min, the valves were reversed and 800 mL was transferred back from B to A. This process was continued for the duration of the treatment period. As demonstrated in Fig. S2, the recirculation of the disinfectant solution was also

setup to perform automatically by a pre-programed timer/control box with multiple start and stop times per day aimed at achieving the proposed operational instructions.

After 3 days of nanosilver treatment, the dental tubing was transferred back to the continuous water flow system following the procedure used in dentist offices. Microbial analysis of the dental tubing was performed immediately after the 3 days of nanosilver treatment. A 1 ft segment of dental tubing was cut into 6 sections and each section was sliced in half for microbial analysis. The biofilm was removed from the sectioned pieces of the tubing by means of either physical scraping or sonication. Biofilm collection by scraping was done by scooping the biofilm using disposable inoculating loops. As for sonication, the sliced tubing sections were immersed in centrifuge tubes containing 30 mL sterile water and sonicated for an interval of 10 min (Fisher Scientific, Ultrasonic Cleaner, FS30, 100w, 40 kHz). Sonication was proven to be a more effective way for removal and/or re-suspensionof biofilms and bacteria in sterile water compared to other physical methods such as scraping (Gagnon and Slawson, 1999, Manuel et al., 2007, Jost et al., 2014). The water samples collected after following sonication were filtered through 0.4 μm polycarbonatefilters. Subsequently, the water samples were plated onto R2A agar in 10, 100 and 1000 fold dilutions and incubated for 1 week at 25 °C on duplicate plates. The R2A plates were evaluated for colonies after one week. Colonies were counted and recorded as colony forming units, CFU ml^{-1}.

Transmission electron microscopy (TEM, JEOL JSM 2100), Scanning electron microscopy(SEM, JEOL JSM 6490LV and JEOL JSM 7600F) and Energy-dispersive X-ray analysis(EDX, Oxford Isis) were used for characterization of the nanosilver and biofilm, respectively. For TEM analysis, samples were prepared by depositing a drop of nanoparticle suspension onto a carbon coated copper grid and air-drying the samples at room temperature in a dust-free box overnight. For SEM characterization, the dental tubing samples were cut and placed in 2.5% gluteraldehyde in 0.1 M cacodylate buffer. Afterwards, samples were placed in 1% OsO_4 and washed with double distilled water, dehydrated in a dilution series of ethanol-water solution and placed in a desiccator to be air-dried. Subsequently, samples were mounted and gold coated for examination with SEM. Finally, an elemental composition analysis of the silver nanoparticles by energy-dispersive X-ray spectroscope (EDX, Oxford Isis) was performed to confirm the elemental presence of silver in the electron micrographs.

Prior to the initialization of the experiment, evaporated (concentrated) pristine Ag nanoparticles were suspended in distilled water and subsequently evaporated in droplets onto a sticky carbon tape and placed on the platen for X-ray photoelectron spectroscopy (XPS) analysis. Surface elemental speciation and composition of the pristine silver nanoparticles was performed using XPS (Scanning Al-Kα source). The binding energy was set in the region of 0–1450 eV and the resolution <0.5 eV using beam width resolution of 10–100 μm. The analysis took place in High Power mode with neutralization (anti-charging) by electrons and argon ions. Further details of the XPS analysis can be found in the SI.

To evaluate transformations in silver speciation that may have occurred in the course of the disinfection process, X-ray absorption spectroscopy (XAS) was conducted at Sector 10-ID (Segre et al., 2000) of the Advanced Photon Source of Argonne National Laboratory (ANL),

Argonne, IL following the experimental setup and sample analysis described by Lombi et al. (2013). Upon completion of the disinfection process, the used nanosilver solution was collected and stored in a dark serum bottle to prevent changes in speciation. In order to reach detectable silver concentrations, a 50 mL aliquot of the spent nanosilver solution was filtered through a 0.45 μm polycarbonate membrane, and the membrane was dried overnight in an anaerobic chamber. The AgNPs accumulated on the membrane were examined by XAS utilizing a quick scan set up.

3. Results and discussion

3.1. Microbial analysis

Table S1 shows the bacterial growth in CFU ml^{-1} for the dental tubing samples after 2 weeks, 1 month, 10 weeks, 3.5 months and 5.5 months of continuous tap water flow. According to the results, there were no detectable bacterial developments on the inner surface of the dental tubing during the initial 2 weeks. Microbial analysis of triplicate tap water samples indicated negligible CFU counts, theoretically explaining the lack of significant biofilm formations in the first few weeks. The first indications of bacterial growth in the tubing came after 3.5 months of continuous water flow. Although it has been reported the CFU levels can reach magnitudes of 10^5 after one or two weeks (Walker et al., 2003, Porteous et al., 2013), results from other experiments show a lower CFU level and biofilm growth comparable to our study (Schel et al., 2006, Porteous et al., 2011). Variations in the CFU measure, as well as biofilm density may be caused by dissimilar planktonic bacterial levels present depending on the water quality. As demonstrated in Table S1, the bacterial growth increases over time and after 5.5 months of tap water flowing through the lines, the CFU count is in the order of 10^2–10^3 for the dental tubing.

Table S2 shows the data pertaining to the microbial analysis (CFU/ml) of the dental tubing surface before and after the nanosilver disinfection process. As demonstrated, upon treatment with the nanosilver suspension, no CFU were detected on the dental tubing surface. Nevertheless, it must be emphasized that the CFU count is presented as general confirmation of the occurrence of the disinfection process, while the primary goal of this study was to evaluate the potential physicochemical alterations of the AgNPs.

3.2. Scanning electron microscopy (SEM)

Fig. 1 shows SEM images of the inner surface of pristine dental tubing. Dust-like material and particles can be observed on the large-view image Fig. 1A. The soft texture of the polyurethane surface can be clearly seen in Fig. 1B. The polyurethane inner surface of dental tubing is a favorable substrate for microbial attachment and growth (Walker and Marsh, 2007). Fig. 2A and B displays the SEM images of the inner surface of the tubing after 19 days and 4 months of continuous tap water flow, respectively. In Fig. 2A, the biofilm is covered by extracellular polymeric substance (EPS), a slime-like matrix that gives biofilm stability and helps it adhere to the tubing surface (Hall-Stoodley et al., 2004). The EPS development at this stage is very thin; however, several rod shaped bacteria can be detected in the biofilm development. The biofilm structure may still be in its early stages of development at this point. In Fig. 2B, relative progression of the biofilm growth is evident

and an increase in the bacteria population is noticeable within the EPS compared to Fig. 2A. However, an overview SEM image of the same area of the tubing indicates the biofilm growth to be sporadic with low density at this time point. This may potentially explain the relatively low CFU counts encountered in Table S1.

Fig. 3A and B displays the backscattered and secondary electron SEM of the same area of the biofilm surface after treatment with nanosilver. As a result, the particle spatial distributionis consistent on both SEM images. Distinct bright particles are observed on the surface of the biofilm in Fig. 3A. In view of the fact that backscattered SEM imaging is capable of displaying distinguishable contrasts amongst different materials, it is our opinion that the bright distinctive particles visible in Fig. 3A are silver in the form of particles or aggregates. This hypothesis was further established by detection of a large particle on the biofilm surface using high magnification backscattered SEM imaging in Fig. S3.

3.3. Transmission electron microscopy (TEM) and energy-dispersive X-ray (EDX) analysis

The TEM image of the pristine commercial ASAP-AGX-32 nanosilver is shown in Fig. 4A. The pristine AgNPs are small in size, ranging between 3 and 5 nm in diameter, spherically shaped and surrounded by a polymer. The corresponding EDX spectrum, however, distributes a weak Ag signal as can be seen in Fig. 4B. The weak EDX signal is perceived to be related to the small size of the particles and the existence of the surrounding polymer. The utilization of a polymer is primarily known to be for stabilization of AgNPs in aqueous solutions (Iravani et al., 2014). Although the composition of the specific polymer used in this commercial product is not specified by the vendor, TEM images of comparable polymers and particles surrounded by polymers have been previously reported (Brown et al., 2007, El-Shall et al., 2009, Liu et al., 2009, Xing et al., 2009). As an example, Brown et al. presents time-resolved, in situ TEM imagery, demonstrating real-time alterations to the polymer on a TEM grid (Brown et al., 2007). El-Shall et al. presents TEM images of metallic and bimetallic particles bound and stabilized by polymers (El-Shall et al., 2009). All of the reported TEM imaging demonstrate a polymer morphology similar to that depicted in Fig. 4A. Furthermore, the existence of a strong carbon peak indicates the presence of a stabilizing agent in the prepared EDX samples (Fig. 4B).

To monitor the physical transformations that AgNPs may potentially encounter during the course of the disinfection process, further TEM imaging was performed. Fig. 5A and C displays TEM images of the AgNPs subsequent to recirculation through the dental tubing for 3 days (disinfection process). It is evident that the pre-existing polymer encapsulating the silver nanoparticles are no longer present. The polymer may have adsorbed onto the surface of the dental tubing or biofilm during the treatment period. The corresponding EDX spectra displayed in Fig. 5B (after disinfection process) is focused on a non-aggregated portion of the AgNPs, and demonstrates an Ag signal similar to that of Fig. 4B (pristine). Although the EDX analysis was performed using similar spot size, it is probable that different locations may contain different numbers of particles leading to an altered Ag signal strength. The absence of the polymer as a stabilizer appears to have initiated the aggregation of a proportion of the AgNPs, as shown in Fig. 5C. Although a fraction of the AgNPs have lost their stability in suspension, forming larger aggregated particles, small particles in the 3–5

nm range are still dominant in number. Fig. 5D is the EDX spectrum corresponding to the aggregate particles (Fig. 5C). This spectrum displays a considerably strong Ag signal, which is attributed to the accumulation of particles forming the aggregate. The observed aggregated Ag particles measured between 50 and 200 nm in diameter. This considerable increase in particle size observed in Fig. 5D impacts the physicochemical properties of the AgNPs, giving rise to different environmental impacts and transportation scenarios (after disposal) compared to the pristine AgNPs (Agnihotri et al., 2014). As an example, aggregated silver nanoparticles are less stable compared to the pristine nanoparticles' containing the polymer stabilizer, and consequently, more likely to precipitate out of solution. In addition, particle aggregation causes a decrease in surface area, lowering their surface of contact (reactivity), and therefore lowering their antimicrobial capabilities (Yu, 2007, Dorjnamjin et al., 2008, Kvitek et al., 2008, Li and Lenhart, 2012).

3.4. Silver speciation by X-ray photoelectron spectroscopy (XPS) and X-ray absorption spectroscopy (XAS)

To determine the chemical speciation state of the particles in the pristine nanosilver solution, XPS measurements at the Ag 3d core levels were conducted. Previous studies have demonstrated the $Ag3d_{5/2}$ binding energies for Ag, Ag_2O and AgO are approximately 368.2, 367.8 and 367.4 eV, respectively (Lai et al., 2010, Prieto et al., 2012). The Ag $3d_{5/2–3/2}$spectrum is shown in Fig. 6, with binding energies of Ag3d doublet peaks located at 367.7 ($Ag3d_{5/2}$) and 373.7 ($Ag3d_{3/2}$) eV. Comparison of these peaks with the 3d peaks available from Ag metal (BE = 368.0 eV) reveals some major differences. The binding energy of Ag3d core levels for the pristine nanosilver solution shifts towards lower binding energy values signifying the existence of silver oxidation states. Therefore, according to the peak shifts of the Ag3d lines observed between both species (i.e. an Ag $3d_{5/2}$ peak at 367.05 ± 0.05 eV and a $3d_{3/2}$ peak at 373.25 ± 0.05 eV), the presence of Ag^{3+} ions is likely. According to the literature and our experiments, the binding energy of the $3d_{5/2}$ level is equal to 368.3 ± 0.1 eV for silver metal, and that of Ag_2O (i.e. Ag^{+1}) is about 367.9 ± 0.1 eV; therefore, a shift of about 0.3 eV per valence unit to lower energies can be expected. Thus, the measured value of 367.3 eV measured for this peak is well in accordance with the presence of Ag^{3+} ions in the oxide layer (Lutzenkirchen-Hecht and Strehblow, 2009, Ferraria et al., 2012). Further analysis of the spectrum indicates the pristine nanosilver solution to be comprised of AgO (~74%) with a small admixture of Ag (I) and Ag (III) (~26%).

Previous studies indicate transformation of AgNPs to AgCl to be anticipated when exposed to chloride containing environments (Gitipour et al., 2013). The XAS spectra from the analysis of the nanosilver solution after the disinfection process is demonstrated in Fig. 7A. A visual inspection of Fig. 7A demonstrates AgCl as the dominant species developed following the disinfection process. In fact, analysis of the LCF results (Fig. 7B) indicates that the dominant species formed were AgCl. As tap water contains fairly high levels of chlorine, the formation of AgCl was triggered and anticipated. Therefore, under the current conditions present in the DUWL disinfection system, phase transformations of AgNPs are likely. Phase transformations are of importance as they may impact the stability, bioavailability and toxicity of AgNPs.

4. Conclusion

In summary, this research highlights the physicochemical alterations, as well as fate of the commercial AgNPs, during dental tubing disinfection process. The analysis of colony forming units (CFU/ml) for the dental tubing, before and after treatment, demonstrates a decrease in the CFU count, and confirms the occurrence of the disinfection process. Characterization of the commercial nanosilver revealed the pristine AgNPs to be spherical in shape, ranging between 3 and 5 nm in size, and bound by a stabilizing polymer. However, after disinfection, the polymeric stabilizing agent surrounding the AgNPs were no longer visible. The disappearance of the polymer was most likely due to adsorption onto the biofilm surface. As a result of the absence of the capping agent, aggregation of a fraction of the silver nanoparticles were initiated. The AgNP aggregates size distribution ranged between 50 and 200 nm in diameter. Additionally, surface transformations of the silver nanoparticles were observed after the course of the disinfection process (treatment process). The pristine nanoparticles were demonstrated through XPS analysis to be dominantly silver oxides (AgO) with a miniscule portion of Ag (I) and Ag (III) while the spent nanosilver solution displayed substantial surface transformations of the AgNPs to AgCl.

To the best of our knowledge, this manuscript demonstrates the first time Ag nanoparticles have been demonstrated to adsorb onto biofilm surfaces. This work can be an initial step in better understanding how nanomaterials, specifically AgNPs, transform depending on the conditions they are exposed to during their usage scenario. Until this date, most research has been focused on assessing the impacts of pristine nanomaterials on various systems. However, it is our belief that nanoparticles may go through transformations during their lifecycle that must be taken into consideration prior to making judgements in regards to their environmental toxicity (natural or engineered systems).

Supplementary Material

Refer to Web version on PubMed Central for supplementary material.

Acknowledgements

This research was performed and funded by the USEPA's National Risk Management Research Laboratory, Cincinnati, Ohio. This paper has been subjected to the Agency's internal review and quality assurance approval. The views and conclusions presented herein do not reflect the views of the Agency or its policy. This research was conducted under the USEPA's Office of Research and Development Chemical Safety for Sustainability Program. Any mention of products or trade names does not constitute a recommendation for use by the USEPA.

References

Agnihotri S; Mukherji S; Mukherji S Size-controlled silver nanoparticles synthesized over the range 5–100 nm using the same protocol and their antibacterial efficacy. RSC. Adv 2014, 4, 3974–3983.

Blake GC The incidence and control of bacterial infection of dental units and ultrasonic scalers. Brit Med J. 1963, 115, 413–416.

Brown RM; Barnes Z; Sawatari C; Kondo T Polymer manipulation and nanofabrication in real time using transmission electron microscopy. Biomacromolecules 2007, 8, (1), 70–76. [PubMed: 17206790]

Correa JM; Mori M; Sanches HL; da Cruz AD; Poiate E, Jr.; Poiate IA Silver nanoparticles in dental biomaterials. Int J Biomater. 2015, 485275. [PubMed: 25667594]

Costa D; Girardot M; Bertaux J; Verdon J; Imbert C Efficacy of dental unit waterlines disinfectants on polymicrobial biofilm. Water Res. 2016, 91, 38–44. [PubMed: 26773487]

Donoso-Bravo A; Mailier J; Martin C; Rodriguez J; Aceves-Lara CA; Wouwer AV Model selection, identification and validation in anaerobic digestion: a review. Water Res. 2011, 45, 5347–5364. [PubMed: 21920578]

Dorjnamjin D; Ariunaa M; Shim YK Synthesis of silver nanoparticles using hydroxyl functionalized ionic liquids and their antimicrobial activity. Int. J. Mol. Sci 2008, 9, (5), 807–819. [PubMed: 19325785]

El-Shall MS; Abdelsayed V; Khder A; Hassan HMA; El-Kaderi HM; Reich TE Metallic and bimetallic nanocatalysts incorporated into highly porous coordination polymer MIL-101. J. Mater. Chem 2009, 19, (41), 7625–7631.

Ferraria A; Carapeto A; Botelho do Rego A X-ray photoelectron spectroscopy: Silver salts revisited. Vacuum. 2012, 86, 1988–1991.

Gagnon GA; Slawson RM An efficient biofilm removal method for bacterial cells exposed to drinking water. J. Microbiol. Methods 1999, 34, (3), 203–214.

Gitipour A; ElBadawy A; Arambewela M; Miller B; Scheckel K; Elk M; Ryu H; Gomez VA; Santo Domingo J; Thiel S; Tolaymat T The impact of silver nanoparticles on the composting of municipal solid waste. Environ. Sci. Technol 2013, 47, 14385–14393. [PubMed: 24143996]

Hajipour MJ; Fromm KM; Ashkarran AA; de Aberasturi DJ; de Larramendi IR; Rojo T; Serpooshan V; Parak WJ; Mahmoudi M Antibacterial properties of nanoparticles. Trends Biotechnol. 2012, 30, (10), 499–511. [PubMed: 22884769]

Hall-Stoodley L; Costerton JW; Stoodley P Bacterial biofilms: From the natural environment to infectious diseases. Nat. Rev. Microbiol 2004, 2, (2), 95–108. [PubMed: 15040259]

Iravani S; Korbekandi H; Mirmohammadi SV; Zolfaghari B Synthesis of silver nanoparticles: chemical, physical and biological methods. Res. Pharm. Sci 2014, 9, (6), 385–406. [PubMed: 26339255]

Jost GF; Wasner M; Taub E; Walti L; Mariani L; Trampuz A Sonication of catheter tips for improved detection of microorganisms on external ventricular drains and ventriculo-peritoneal shunts. J. Clin. Neurosci 2014, 21, (4), 578–582. [PubMed: 24326253]

Kvitek L; Panacek A; Soukupova J; Kolar M; Vecerova R; Prucek R; Holecova M; Zboril R Effect of surfactants and polymers on stability and antibacterial activity of silver nanoparticles (NPs). J. Phys. Chem 2008, 112, (15), 5825–5834.

Lai Y; Zhuang H; Xie K; Gong D; Tang Y; Sun L; Lin C; Chen Z Fabrication of uniform Ag/TiO_2 nanotube array structures with enhanced photoelectrochemical performance. New. J. Chem 2010, 34, 1335–1340.

Li X; Lenhart JJ Aggregation and dissolution of silver nanoparticles in natural surface water. Environ. Sci. Technol 2012, 46, (10), 5378–5386. [PubMed: 22502776]

Liu JF; Liu R; Yin YG; Jiang GB Triton X-114 based cloud point extraction: a thermoreversible approach for separation/concentration and dispersion of nanomaterials in the aqueous phase. Chem. Commun 2009, (12), 1514–1516.

Lombi E; Donner E; Taheri S; Tavakkoli E; Jamting AK; McClure S; Naidu R; Miller BW; Scheckel KG; Vasilev K Transformation of four silver/silver chloride nanoparticles during anaerobic treatment of wastewater and post-processing of sewage sludge. Environ. Pollut 2013, 176, 193–197. [PubMed: 23434771]

Lutzenkirchen-Hecht D; Strehblow H Anodic silver (II) oxides investigated by combined electrochemistry, ex situ XPS and in situ X-ray absorption spectroscopy. Surf. Interface Anal 2009, 41, 820–829.

Manuel CM; Nunes OC; Melo LF Dynamics of drinking water biofilm in flow/non-flow conditions. Water Res. 2007, 41, (3), 551–562. [PubMed: 17184812]

Pankhurst CL; Coulter W; Philpott-Howard JN; Surman-Lee S; Warburton F; Challacombe S Evaluation of the potential risk of occupational asthma in dentists exposed to contaminated dental unit waterlines. Primary Dental Care: Journal of the Faculty of General Dental Practitioners (UK) 2005, 12, (2), 53–9. [PubMed: 15901433]

Pankhurst CL; Johnson NW; Woods RG Microbial contamination of dental unit waterlines: the scientific argument. Int Dent J 1998, 48, (4), 359–68. [PubMed: 9779119]

Porteous N; Luo J; Hererra M; Schoolfield J; Sun YY Growth and identification of bacterial in N-halamine dental unit waterline tubing using an ultrapure water source. Int. J. Microb 2011, 767314.

Porteous N; Sun YY; Dang SC; Schoolfield J A comparison of 2 laboratory methods to test dental unit waterline water quality. Diagn. Microbiol. Infect. Dis 2013, 77, (3), 206–208. [PubMed: 24054735]

Prieto P; Nistor V; Nouneh K; Oyama M; Abd-Lefdil M; Diaz R XPS study of silver, nickel and bimetallic silver-nickel nanoparticles prepared by seed-mediated growth. Appl. Surf. Sci 2012, 258, 8807–8813.

Schel AJ; Marsh PD; Bradshaw DJ; Finney M; Fulford AR; Frandsen E; Ostergaard E; ten Cate JM; Moorer WR; Mavridou A; Kamma JJ; Mandilara G; Stosser L; Kneist S; Araujo R; Contreras N; Goroncy-Bermes P; O'Mullane D; Burke F; O'Reilly P; Hourigan G; O'Sullivan M; Holman R; Walker JT Comparison of the efficacies of disinfectants to control microbial contamination in dental unit water systems in general dental practices across the European union. Appl. Environ. Microbiol 2006, 72, (2), 1380–1387. [PubMed: 16461690]

Shearer BG Biofilm and the dental office. J Am Dent Assoc. 1996, 127, (2), 181–9. [PubMed: 8682987]

Shepherd PA; Shojaei MA; Eleazer PD; Van Stewart A; Staat RH Clearance of biofilms from dental unit waterlines through the use of hydroperoxide ion-phase transfer catalysts. Quintessence Int. 2001, 32, 755–761. [PubMed: 11820043]

Szymanska J Biofilm and dental unit waterlines. Ann. Agr. Env. Med 2003, 10, (2), 151–157. [PubMed: 14677905]

The MRCAT Insertion Device Beamline at the Advanced Photon Source", Segre CU, Leyarovska NE, Chapman LD, Lavender WM, Plag PW, King AS, Kropf AJ, Bunker BA, Kemner KM, Dutta P, Duran RSand Kaduk J, CP521, Synchrotron Radiation Instrumentation: Eleventh U.S. National Conference, ed. Pianetta P, et al., p419–422, (American Insitute of Physics, New York, 2000).

Tolaymat TM; El Badawy AM; Genaidy A; Scheckel KG; Luxton TP; Suidan M An evidence-based environmental perspective of manufactured silver nanoparticle in syntheses and applications: A systematic review and appraisal of peer-reviewed scientific papers. Sci. Total Environ 2010, 408, 999–1006. [PubMed: 19945151]

Walker JT; Bradshaw DJ; Fulford MR; Marsh PD Microbiological evaluation of a range of disinfectant products to control mixed-species biofilm contamination in a laboratory model of a dental unit water system. Appl. Environ. Microbiol 2003, 69, (6), 3327–3332. [PubMed: 12788733]

Walker JT; Marsh PD Microbial biofilm formation in DUWS and their control using disinfectants. J. Dent 2007, 35, (9), 721–730. [PubMed: 17714847]

Xing SX; Tan LH; Yang MX; Pan M; Lv YB; Tang QH; Yang YH; Chen HY Highly controlled core/shell structures: tunable conductive polymer shells on gold nanoparticles and nanochains. J. Mater. Chem 2009, 19, (20), 3286–3291.

Yu DG Formation of colloidal silver nanoparticles stabilized by Na+-poly(gamma-glutamic acid)-silver nitrate complex via chemical reduction process. Colloids Surf. 2007, 59 (2), 171–178.

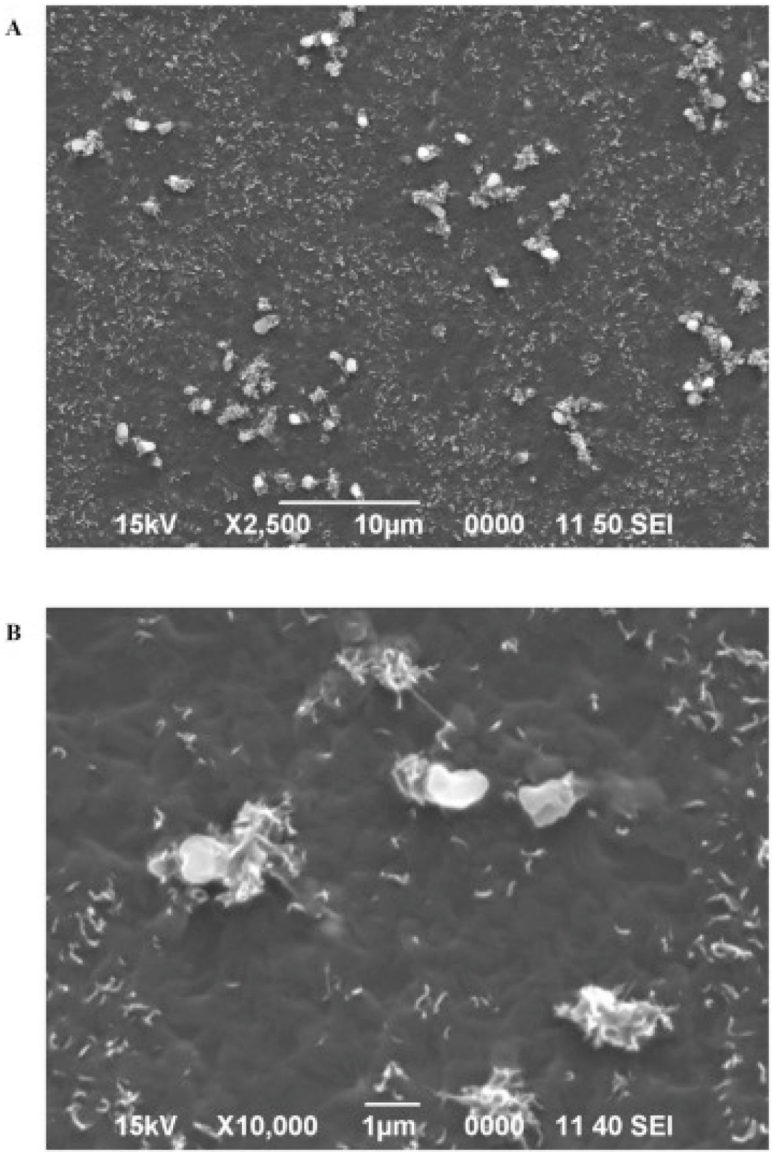

Fig. 1.

SEM images of unused dental tubing surface. Images A) and B) comprise of 2500X view and detailed texture (10,000×) of tubing surface, respectively.

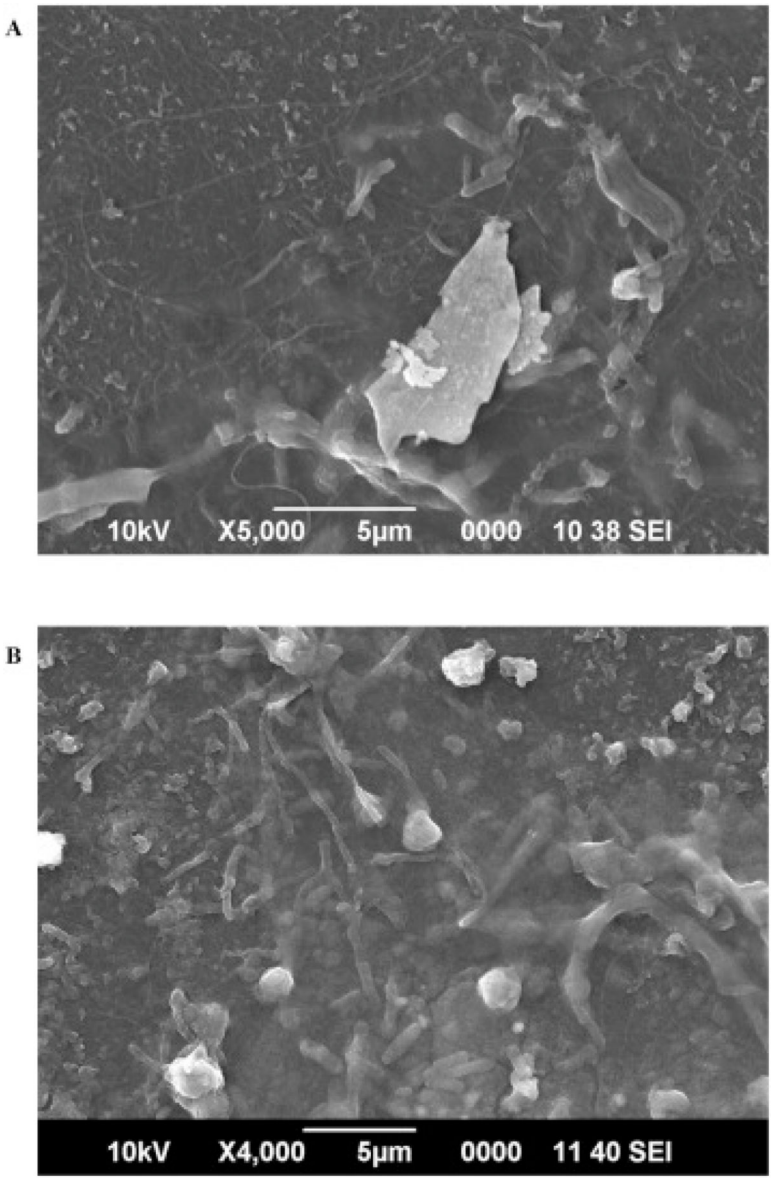

Fig. 2.

SEM image of the biofilm development on the dental tubing surface after (A) 19 days and (B) 4 months of continuous tap water flow.

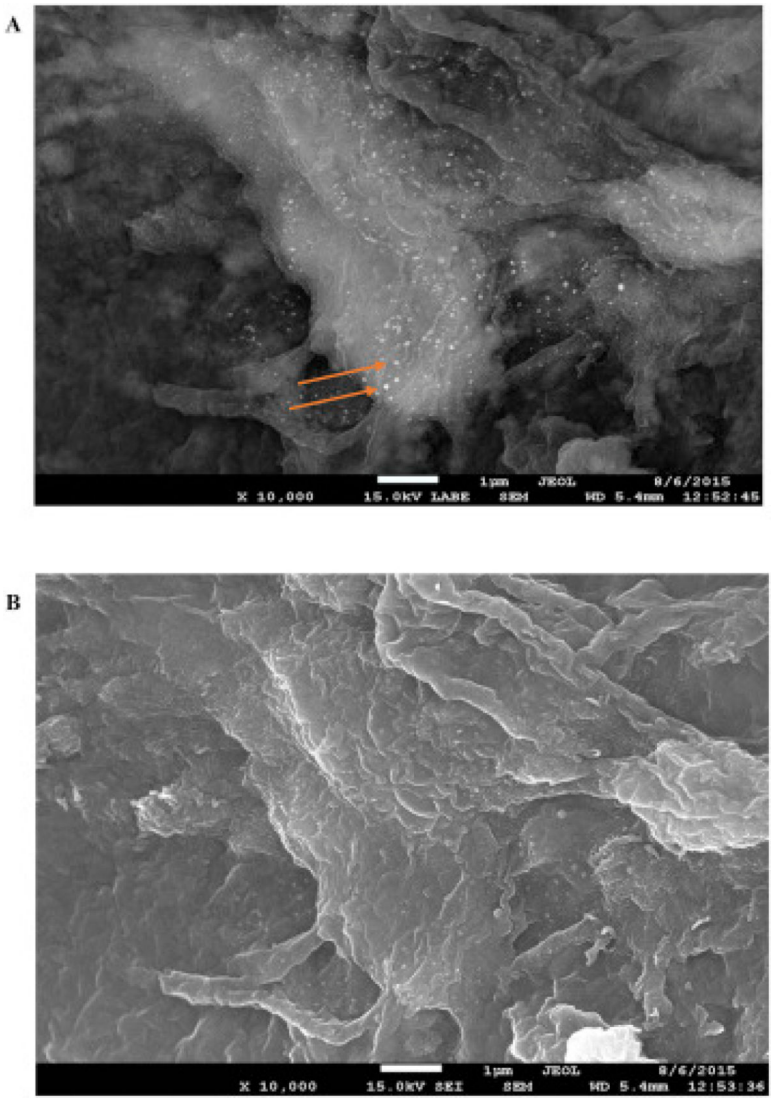

Fig. 3.

(A) Backscattered SEM and (B) secondary electron SEM images of the same area of biofilm. The backscattered SEM image displays the clear contrast between Ag nanoparticles and the surrounding biofilm.

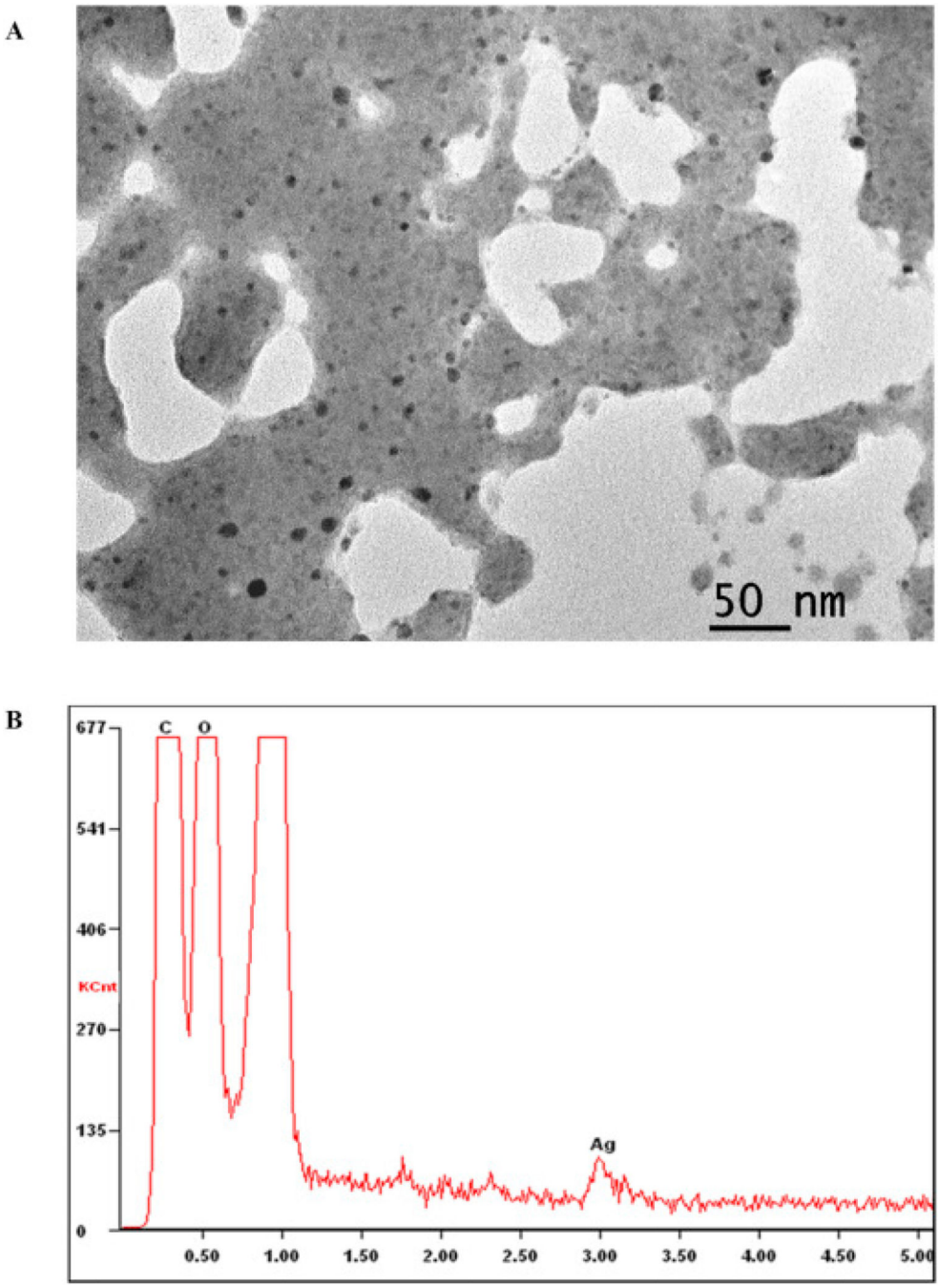

Fig. 4.

(A) TEM image of the pristine ASAP-AGX-32 nanosilver and (B) the corresponding EDX spectrum.

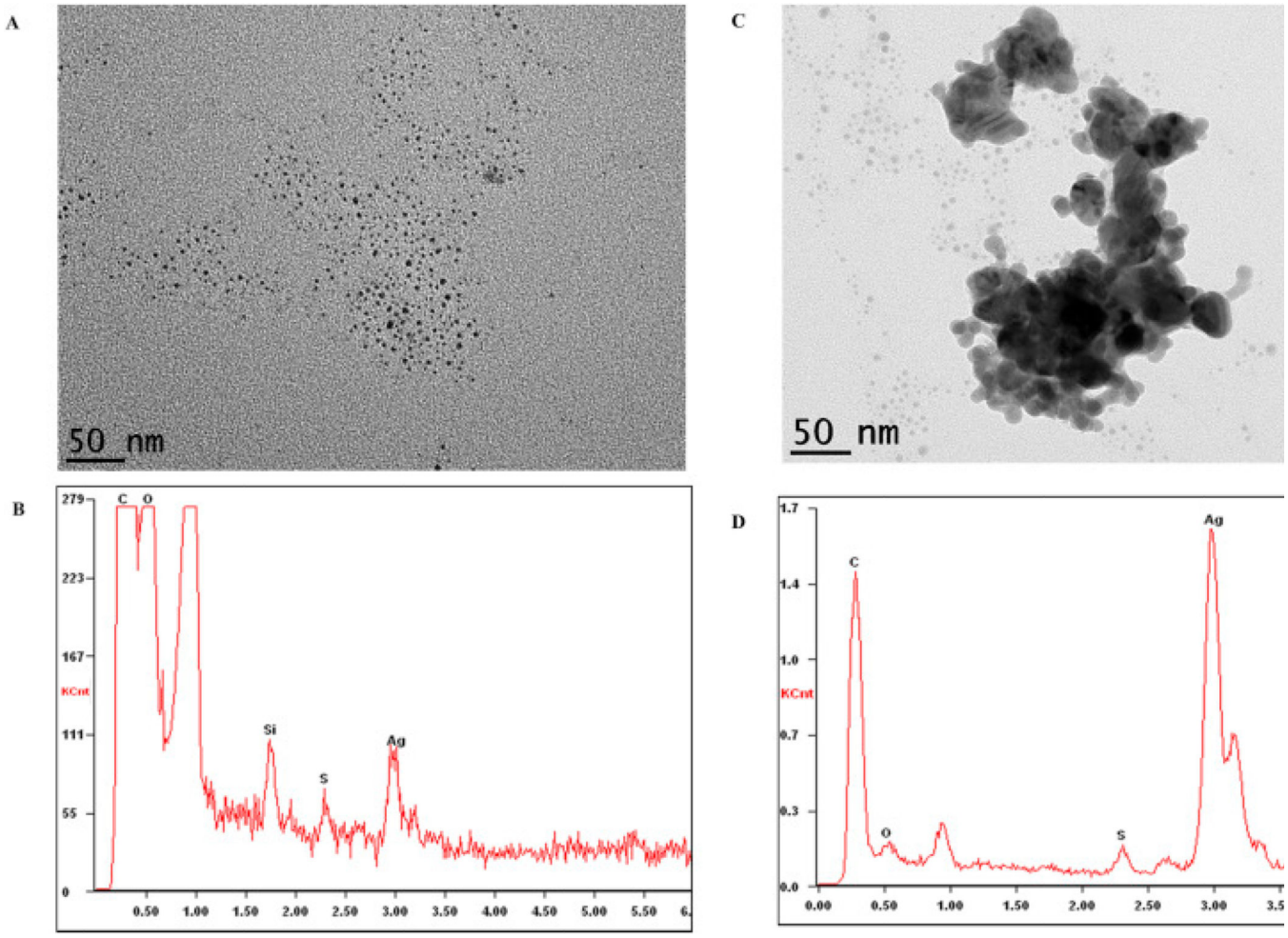

Fig. 5.

(A and C) TEM images of nanosilver after re-circulation through the dental tubing for 3 days. Image A) displays small AgNPs (3–5 nm) and image C) displays a large partially-aggregated Ag particle surrounded by small (3–5 nm) AgNPs. (B and D) are the corresponding EDX spectra of the particles presented in images A and C, respectively.

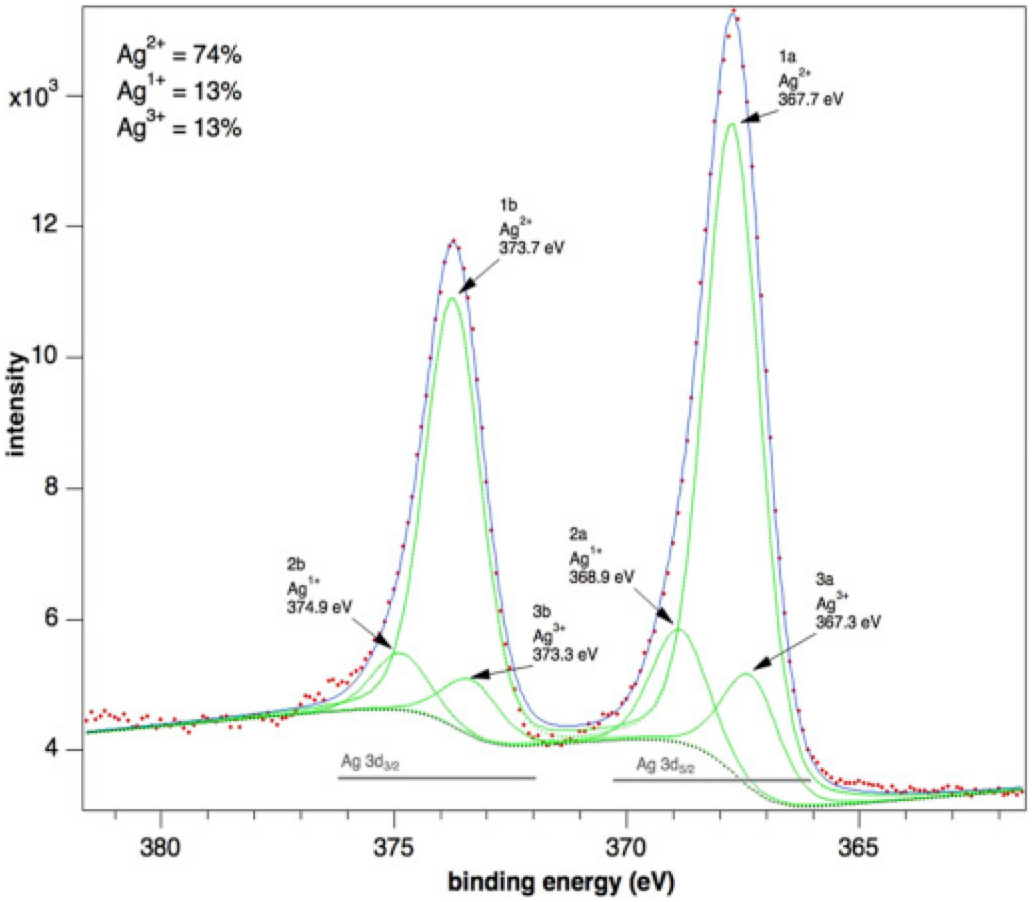

Fig. 6.
AG 3d XPS spectra of pristine Ag nanoparticles.

A)

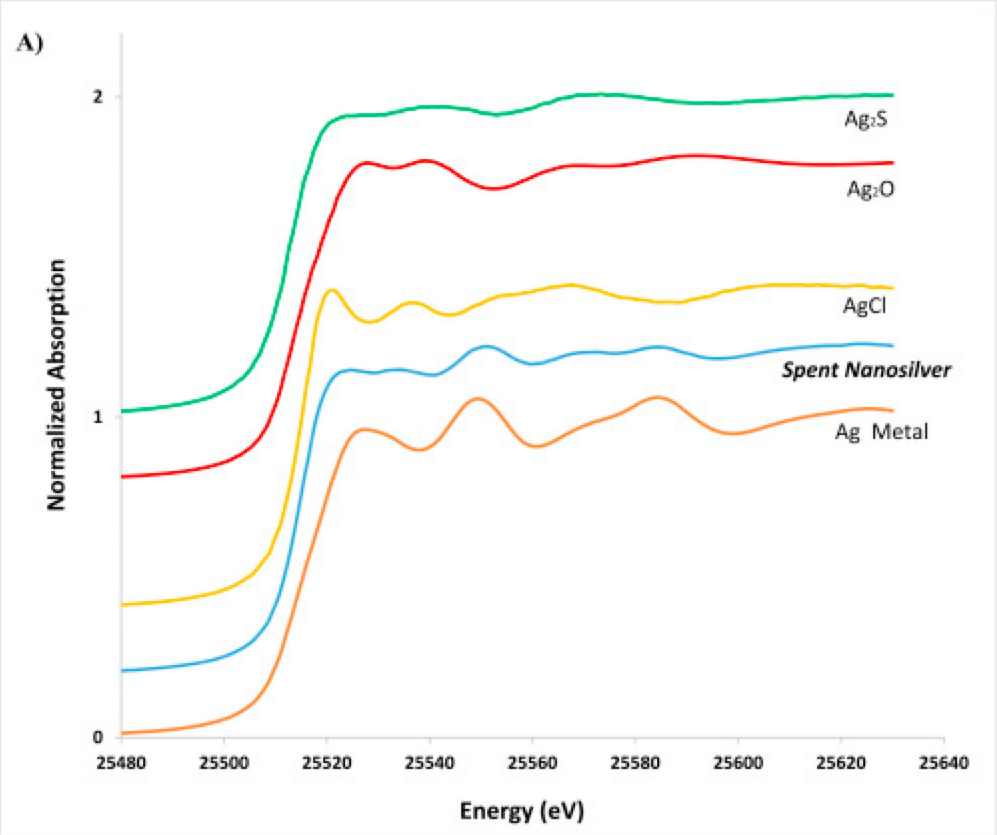

B)

Sample	AgCl (%)	Ag_0 (%)	R-factor (x1000)
Spent Nanosilver	56	44	0.041

Fig. 7.

A) Ag-K_α XAS spectra of Ag_2S, Ag_2O, AgCl and Ag metallic as pure phases and AgNPs (ASAP-AGX-32) after the DUWL disinfection process (Spent Nanosilver). B) Ag speciation as identified by LCF of k-edge XANES spectra. Silver species proportions are presented as percentages. Goodness of fit is indicated by the R-factor.